

Competitive growth of Ta nanopillars during glancing angle deposition: Effect of surface diffusion

C. M. Zhou and D. Gall^{a)}

Department of Materials Science and Engineering, Rensselaer Polytechnic Institute, Troy, New York 12180

(Received 24 July 2006; accepted 16 January 2007; published 20 February 2007)

Periodic arrays of Ta nanopillars were grown onto patterned substrates by glancing angle sputter deposition at growth temperatures T_s ranging from 200 to 900 °C. The Si substrates were patterned using a colloidal suspension of 260-nm-diameter silica spheres that was dispersed to form a two-dimensional close-packed monolayer. At low growth temperatures, $T_s \leq 500$ °C, nanopillars exhibit regular hexagonal arrays. However, the arrays randomize with increasing T_s and completely degrade at $T_s = 900$ °C. The transition to a less ordered film morphology is attributed to strong interpillar competition caused by the increasing adatom diffusion length with increasing T_s . The competitive growth mode leads to a decrease in the pillar number density (by 48%) and pillar separation (from 65 nm to negligible), an increase in the average pillar width from 200 to 260 nm, the accelerated growth of some pillars at the cost of others which die out (25%), and an increased probability (20%) for the merging of neighboring pillars. © 2007 American Vacuum Society. [DOI: 10.1116/1.2539328]

I. INTRODUCTION

Glancing angle deposition (GLAD), also known as oblique angle deposition, is a physical vapor deposition technique in which the incident flux impinges onto the substrate from a glancing angle $\alpha \geq 80^\circ$, resulting in highly underdense columnar thin film microstructures due to atomic shadowing effects during growth. Manipulating both the deposition angle α and the substrate rotation angle φ provides unique flexibility for nanostructure shaping. GLAD has been employed to create nanopillars,¹⁻⁴ zigzags,⁵ nanospirals,⁶⁻⁸ and Y shapes⁹ with engineered optical,¹⁰⁻¹² mechanical,¹³⁻¹⁶ magnetic,¹⁷⁻²⁰ and electrical^{21,22} properties, and potential applications as photonic crystals,⁶⁻⁸ sensors,^{22,23} catalyst support,^{24,25} magnetic storage media,¹⁷⁻²⁰ and field emitters.^{26,27}

The growth competition between neighboring columns plays a critical role during GLAD and strongly affects microstructural evolution, surface morphology, and, in turn, physical properties. Deposition on flat substrates yields column nucleation at random locations, followed by a highly competitive growth mode where the combination of nonuniform column size and atomic shadowing causes broadening and extinction of neighboring columns, as observed by both simulations and experiments.^{28,29} These results also indicate that the layer density is constant with respect to the column height h . That is, the broadening of the column width w , which follows a power law $w \propto h^p$ with a growth exponent p ,³⁰ is compensated by columns that die out, so that the ratio of the mean column width to the mean column separation remains constant.²⁸ However, increasing the deposition angle α leads to an increase in the degree of intercolumnar competition and a decrease in film density.²⁸

Additional insight into column competition during GLAD has been obtained by growth studies on prepatterned substrates fabricated using colloidal self-assembly,^{6,31} embossing techniques,³² and e-beam and laser interference lithographies.^{4,29,33} The patterned surface mounds are nucleation sites for GLAD columns since film growth on the surrounding substrate is suppressed if the ratio between the mound interspacing to its height is less than $\tan(\alpha)$.^{29,33} The resulting GLAD layers exhibit regular arrays of columns, indicating that intercolumnar competition is delayed for growth on prepatterned substrates.^{4,31,33} The competitive growth mode, as revealed and quantified by the extinction of some columns, is further delayed if the period of the patterned array is increased,²⁹ leading to negligible intercolumnar competition and, in turn, regular arrays of columns that are several micrometers tall.^{4,29,31}

These reported results suggest that the lateral length scale of the surface morphology, that is, the center-to-center intercolumnar spacing, determines if the columnar growth is competitive. In addition, column competition is expected to be also affected by the adatom mobility,³⁴ as high adatom mobility materials are reported to form denser films and columns with larger widths than low mobility materials.^{30,35} However, little is known to what extent the adatom surface diffusion length controls the intercolumnar competition during GLAD.

This article describes the growth and characterization of Ta nanopillar arrays grown at temperatures T_s ranging from 200 to 900 °C, with the goal to provide data on the relationship between the surface diffusion length (as controlled by T_s) and the columnar competition during GLAD. All nanopillar arrays were grown by ultrahigh vacuum magnetron sputtering on Si(001) substrates which were patterned with a monolayer of 260-nm-diameter silica nanospheres. Low temperature growth yields nanopillars that exhibit regular hex-

^{a)}Electronic mail: galld@rpi.edu

agonal close-packed arrays. However, as the deposition temperature increases, the arrays randomize and ultimately completely degrade at $T_s=900$ °C. The transition to a disordered film morphology, including an increased pillar diameter and a decreased pillar number density, is attributed to a strong competitive growth mode at elevated temperatures which is caused by an increased adatom diffusion length.

II. EXPERIMENTAL PROCEDURE

Substrates were patterned using 260-nm-diameter silica nanospheres that self-assemble from colloidal suspensions according to the following procedure, modified from Ref. 36. Si(001) substrates were first treated with a boiling piranha solution [H_2SO_4 (98%) and H_2O_2 (30%), volume ratio of 4:1] to obtain a clean and hydrophilic surface, followed by cleaning in an ultrasonic bath of de-ionized water. A dispersion of silica nanospheres (Bangs Laboratories, Inc., 10 wt %) was diluted in de-ionized water with a ratio of 1:40. A 40 μl droplet of this colloidal suspension was deposited on the substrates that were tilted by 6° off the horizontal and placed in a glass chamber containing an ice-water bath. The chamber protects the surface from external air flow and allows, with the use of the ice-water bath, to provide a controlled reproducible temperature and humidity environment for slow evaporation. The inclination yields a gradient in the depth of the droplet and results in a monotonic drying from top to bottom, leaving a close-packed monolayer of nanospheres.

All Ta nanocolumn arrays were grown in a load-locked ultrahigh vacuum stainless steel dc magnetron sputter deposition system described in detail in Ref. 31. A 7.5-cm-diameter Ta target (99.95% pure) was positioned 10 cm from the substrate with the target surface perpendicular to the substrate surface. The deposition angle $\alpha=84^\circ$ is controlled by a collimating plate, which also prevents nondirectional deposition flux from impinging onto the substrate. The patterned Si substrates were attached to a molybdenum holder using Pelco colloidal silver paste (Ted Pella, Inc.) and introduced through the load lock into the deposition chamber which has a base pressure of 2×10^{-6} Pa. Ar (99.999% pure) was further purified using a MicroTorr purifier and introduced through metering valves to reach a constant pressure of 0.39 Pa (3 mTorr), which was measured by a capacitance manometer (Baratron) and held constant during all depositions. The growth temperatures, $T_s=200, 300, 500, 700,$ and 900 °C, were controlled by a radiative pyrolytic graphite heater and measured, including the contribution due to plasma heating, by a thermocouple attached to the substrate holder. Sputtering was carried out at a constant power of 500 W, yielding a column growth rate that ranges, depending on the layer density which varies with the growth temperature, from 3.5 to 5.3 nm/min. The substrates were continuously rotated about the polar axis with 60 rpm, resulting in an overall circular symmetric deposition flux. Microstructures were investigated by plan-view and cross-sectional

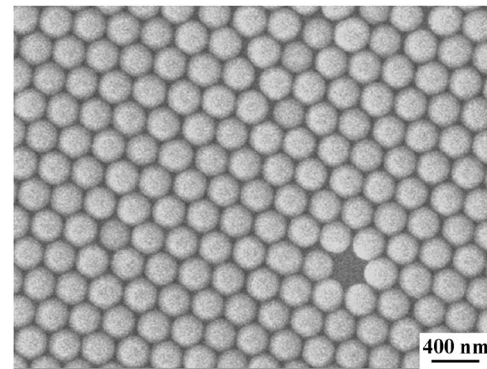


FIG. 1. SEM micrograph of 260-nm-diameter SiO_2 nanospheres on Si(001), forming a self-assembled hexagonal close-packed monolayer including a vacancy defect.

scanning electron microscopy (SEM) using a JEOL JSM6335 field emission SEM operated at 5 kV with an emission current of 12 μA .

III. RESULTS

Figure 1 is a plan-view SEM micrograph showing a typical patterned surface used for subsequent GLAD growth. It shows a Si(001) substrate that is covered with a monolayer of 260-nm-diameter silica spheres. The nanospheres form a regular, hexagonal close-packed array with a measured periodicity of 256 nm, in excellent agreement with the nominal sphere diameter of 260 nm. The micrograph also shows a vacancy defect in the nanosphere array. Large-area analyses show that 3% of lattice sites are vacant, corresponding to a vacancy concentration of $0.5 \mu\text{m}^{-2}$. In addition, the nanosphere layer exhibits one-dimensional crystalline defects such as dislocations and grain boundaries with relatively low densities $<0.25 \mu\text{m}^{-1}$, comparable to what we have reported previously.³⁷ We attribute the defect formation to a combination of the nanosphere polydispersity and kinetic limitations during the drying process. The large-scale structure of the monolayers is a grid of long stripes, 10–60 μm wide and several millimeters long, which are caused by the directional drying process.

Figure 2 shows typical plan-view SEM micrographs from Ta nanopillar arrays grown at $T_s=200, 300,$ and 500 °C by glancing angle sputter deposition on regularly patterned substrates. The nanopillars grown at $T_s=200$ °C in Fig. 2(a) exhibit a hexagonal array with a measured center-to-center pillar distance of 262 ± 15 nm. The nanopillars replicate the arrangement of the silica nanosphere pattern shown in Fig. 1, indicating that each nanosphere leads to the formation of a Ta pillar. The hexagonal arrangement is also observable for layers grown at 300 and 500 °C in Figs. 2(b) and 2(c), respectively; however, the uniformity of the pillar arrangement decreases with increasing T_s . The average pillar widths are $195 \pm 43, 235 \pm 77,$ and 217 ± 64 nm for $T_s=200, 300,$ and 500 °C, respectively, where the error bars correspond to the standard deviation of the width distributions. Some of the pillars are missing, as the one indicated by the dashed square

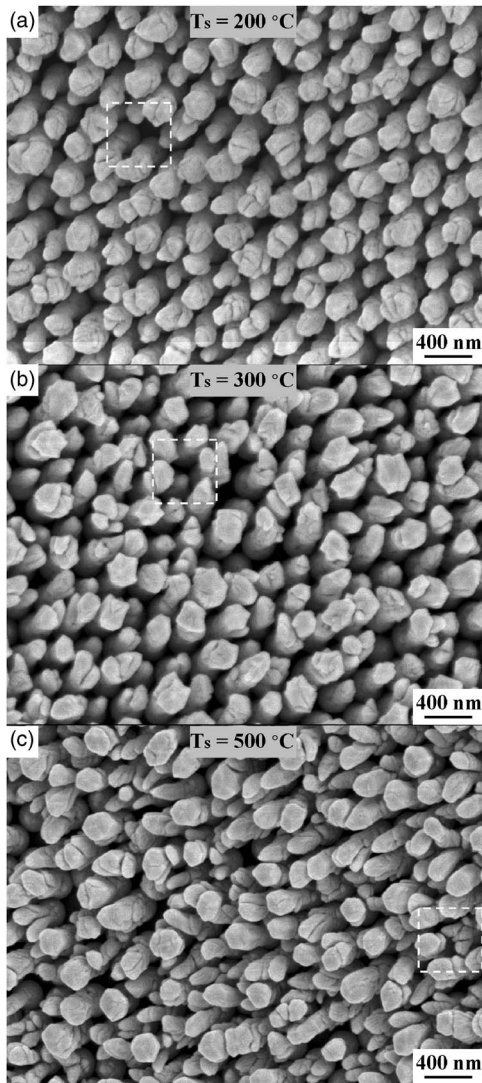


FIG. 2. Plan-view SEM micrographs of Ta nanopillar arrays grown by GLAD on patterned substrates at $T_s=200$, 300, and 500 °C. The dashed squares highlight a missing pillar in (a) and extinct pillars in (b) and (c).

in Fig. 2(a), while others terminate their growth prematurely and die out before growing to their full height, as those highlighted by the dashed squares in Figs. 2(b) and 2(c). The missing pillars are due to vacancy defects in the initial nanosphere patterns, while extinct pillars are attributed to a competitive growth mode between neighboring pillars, as discussed below. The fraction of pillars that die out prematurely increases from 3% to 9% to 34% for $T_s=200$, 300, and 500 °C, respectively. This leads to a corresponding decrease in the nanopillar number density, from 14.9 to 12.7 to $8.6 \mu\text{m}^{-2}$. The micrograph in Fig. 2(a) also shows that the top of some Ta nanopillars splits into two or more subpillars. Large-area analyses indicate that 30% of the pillars are branched at $T_s=200$ °C and that this value decreases with increasing T_s . The branching is attributed to surface roughening on individual pillars which causes self-shadowing and, under limited adatom mobility conditions at low temperatures, leads to the development of subcolumns as discussed in detail in Ref. 38.

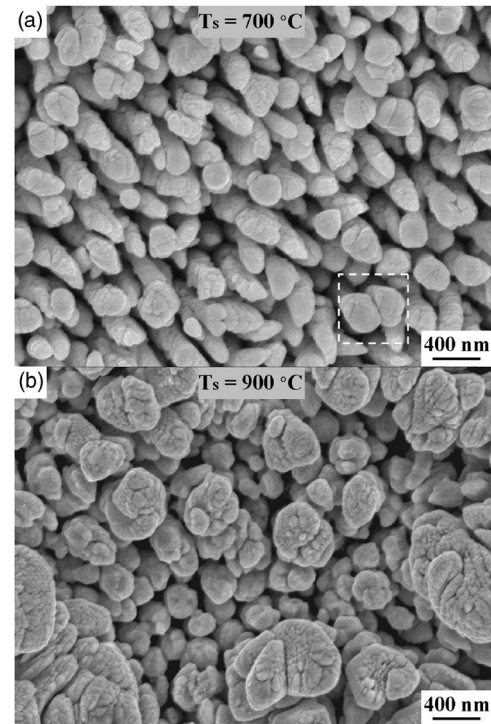


FIG. 3. Plan-view SEM micrographs of Ta nanopillar arrays grown by GLAD on patterned substrates at $T_s=700$ and 900 °C. The dashed square in (a) highlights the merging of two neighboring pillars.

Figures 3(a) and 3(b) are plan-view SEM micrographs for Ta pillar arrays grown under identical conditions, as those shown in Fig. 2, however, at higher temperatures, $T_s=700$ and 900 °C, respectively. The higher growth temperature leads to a randomization of the pillar array for $T_s=700$ °C and a complete degradation into a disordered morphology with large (>500 nm) agglomerates for $T_s=900$ °C. The average pillar width for $T_s=700$ °C is 260 ± 33 nm. This is close to the nominal diameter of the silica spheres of 260 nm and suggests that some pillars may touch each other and may merge as growth continues. The dashed square in Fig. 3(a) highlights two neighboring pillars that touch and would merge into a single pillar if the growth would be continued. Analysis of an $11 \mu\text{m}^2$ area shows that 20% of the nanopillars have merged with one or multiple neighbors. The merging causes a decrease in the pillar number density which, when also accounting for 3% of initial SiO_2 nanosphere vacancies and a measured 25% of pillars that die out due to growth competition, is $7.8 \mu\text{m}^{-2}$ at $T_s=700$ °C.

Figure 4(a) is a corresponding cross-sectional SEM micrograph of Ta nanopillars grown on silica nanospheres at $T_s=200$ °C. The pillars are 630 nm tall and have a measured average width w of 193 ± 14 nm, in good agreement with 195 ± 43 nm, the value obtained from Fig. 2(a). This is considerably smaller than 260 nm, the average column-to-column separation which is controlled by the diameter of the nanospheres, resulting in a 65-nm-wide open space between neighboring pillars. That is, the Ta pillars are well separated, in agreement with the observation from the plan-view micrographs. The pillar width remains approximately constant as a

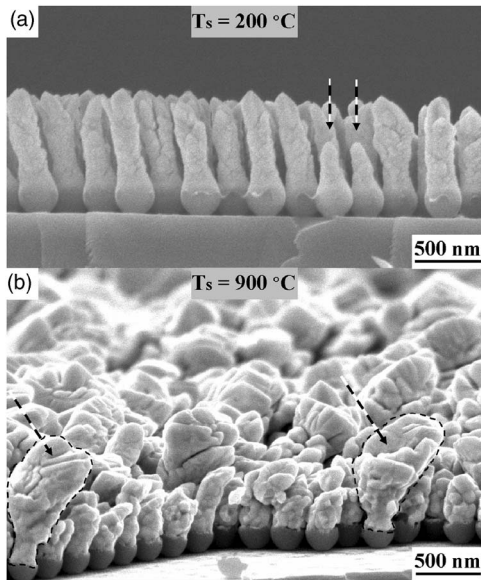


FIG. 4. Cross-sectional SEM micrograph of Ta nanopillar arrays grown at $T_s=200$ and 900 °C. Arrows indicate extinct pillars in (a) and wide pillar heads in (b) (with contours highlighted with dashed lines).

function of height, showing that these columns have been grown without strong intercolumnar competition. The vertical pillar surfaces exhibit considerable roughness which is attributed to kinetic roughening under limited adatom mobility conditions at the relatively low growth temperature. The arrows in Fig. 4(a) highlight two pillars that are shorter than their neighbors. Their premature growth termination is attributed to column competition. However, only a small fraction (3%) of pillars, as determined from plan-view SEM analyses, exhibit such a reduced height, indicating that growth competition is weak at the relatively low T_s of 200 °C.

In contrast, growth at a high temperature, $T_s=900$ °C, leads to broad pillars with an average width of 267 ± 16 nm, shown in Fig. 4(b). This is slightly larger than 260 nm, the nominal diameter of the silica spheres. Consequently, some pillars touch their neighbors, leaving no separation between them. In addition, some pillars exhibit wide heads that protrude out of the array, as those indicated by arrows in Fig. 4(b). Their contours are highlighted by dashed lines. These prominent features correspond to the agglomerates observed in the plan-view micrograph in Fig. 3(b). We attribute the formation of these agglomerates to an exacerbated growth competition between neighboring pillars, initiated by an increased pillar size distribution due to the elevated adatom mobility at high T_s . The large pillars grow at the expense of the surrounding layer which experiences growth suppression. Some agglomerates are the result of the merging of two or multiple pillars which, as a merged feature, capture an overproportional fraction of the deposition flux and dominate in the competitive growth mode.

In addition, the SiO_2 spheres in Fig. 4(b) exhibit a measured diameter of 250 nm, which is 9% below 275 nm, the value observed in Fig. 4(a). We attribute the smaller sphere diameter to a densification upon sintering at the 900 °C

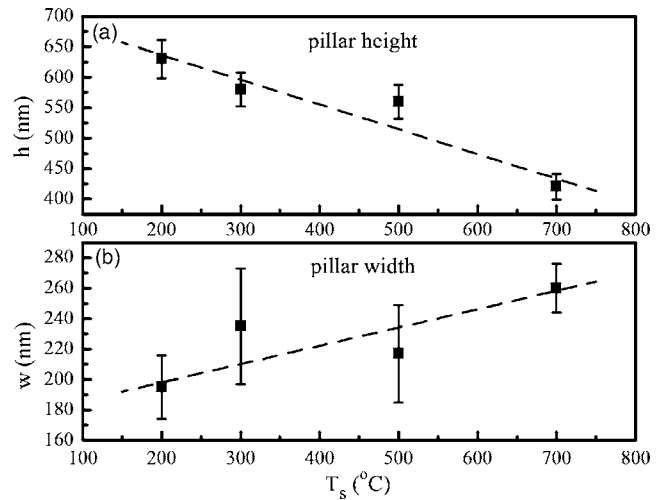


FIG. 5. Plots of (a) average nanopillar height and (b) average nanopillar width as a function of growth temperature, $T_s=200$ – 700 °C. The dashed lines are a guide to the eyes.

growth temperature for 2 h. Similar sphere size reductions by 5%–10% have been previously reported for anneals above the glass transition temperature of ~ 800 °C.^{39,40} The size reduction is attributed to a reduction in the crack sizes which leads to a densification of the spheres. They initially exhibit a density of 2 g/cm³, which is 20% below a fully dense amorphous thermal oxide (2.5 g/cm³). The hexagonal arrangement of the spheres is not affected by the size reduction, as previously reported,⁴¹ and also indicated by the regular arrangement of the spheres in Fig. 4(b). We use, for the following quantitative analysis, only data from Ta rod arrays grown at $T_s \leq 700$ °C, where the shrinkage is expected to be negligible.

Figure 5 shows plots of the average pillar height h and width w as a function of T_s from 200 to 700 °C, as determined from cross-sectional and plan-view micrographs, respectively. The measured height decreases from 630 ± 24 to 420 ± 40 nm, and the width increases from 195 ± 43 to 260 ± 33 nm, as T_s increases from 200 to 700 °C. These changes can be attributed to an increased surface diffusion length at elevated temperatures, as discussed below. The plotted error bars correspond to the standard deviation of the measured values. The slight decrease in average width from 235 ± 77 to 217 ± 64 nm as T_s increases from 300 to 500 °C is due to a transition from single to multiple pillar nucleation per silica nanosphere, as highlighted by dashed squares in Figs. 2(b) and 2(c) and discussed in detail in Ref. 37, resulting in a reduced average width for $T_s=500$ °C.

Figure 6(a) is a plot of the number density of nanopillars as a function of growth temperature T_s . The plot also indicates the measured number density of the hexagonal close-packed array of 260 -nm-diameter silica spheres assuming no vacancies, which is 16.2 μm^{-2} . The nanopillar density decreases monotonically from 14.9 to 12.7 to 8.6 to 7.8 μm^{-2} , as T_s increases from 200 to 300 to 500 to 700 °C, respectively. This decrease is due to the extinction and the merging of some pillars, as quantified in Figs. 6(b) and 6(c), respec-

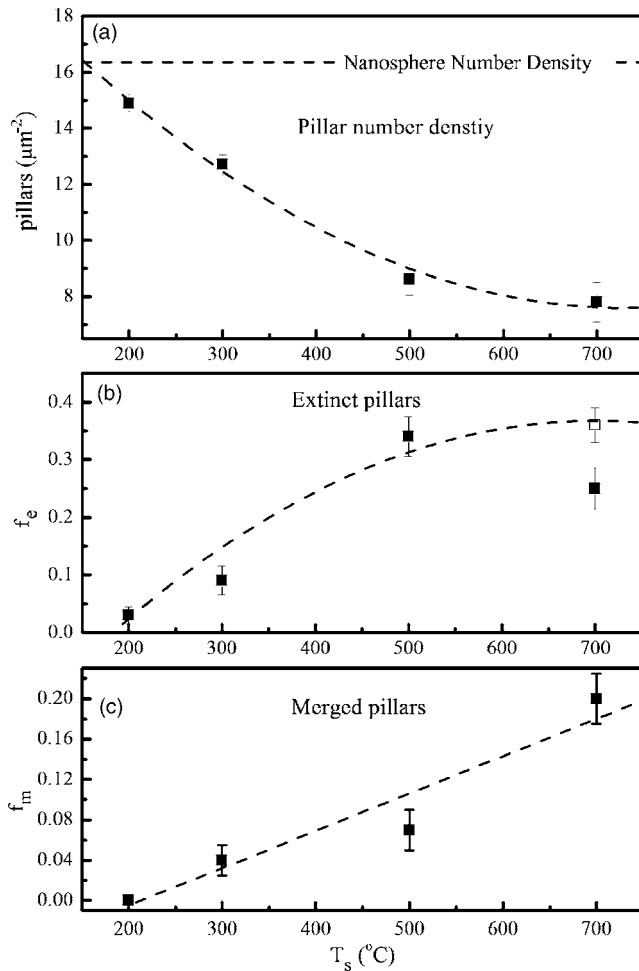


FIG. 6. Plots of (a) the Ta nanopillar number density and (b) the fraction of extinct and (c) of merged pillars, as a function of growth temperature, $T_s=200\text{--}700\text{ }^\circ\text{C}$. The dashed lines are a guide to the eyes.

tively. The fraction f_e of pillars that are extinct is obtained by dividing the measured number density of extinct pillars by the expected number density of pillar nuclei, which is equal to the nanosphere number density. The f_e values increase from 3% at $200\text{ }^\circ\text{C}$ to 34% at $500\text{ }^\circ\text{C}$ and slightly decrease to 25% for $T_s=700\text{ }^\circ\text{C}$. However, if the merged pillars are included in the determination of f_e , by counting half of the merged pillars as extinct, the value for $T_s=700\text{ }^\circ\text{C}$ becomes 35%, as indicated by the open square in Fig. 6(b). For that analysis, f_e increases monotonically with T_s , in agreement with the decreasing pillar number density shown in Fig. 6(a), which is attributed to an increasing competitive growth mode as discussed below. Figure 6(c) is a plot of the fraction f_m of merged pillars as a function of T_s , where f_m is defined as the ratio of pillars that have merged with a neighbor divided by the total number of initial nuclei. The merging is negligible at $T_s=200\text{ }^\circ\text{C}$, but f_m increases with increasing T_s to reach 20% at $700\text{ }^\circ\text{C}$. The increase in f_m is attributed to the increase in w , shown in Fig. 5(b). At $T_s=700\text{ }^\circ\text{C}$, $w=260\pm 33\text{ nm}$, that is, the average pillar width is equal to the nominal diameter of the silica spheres and, in turn, equal to the center-to-center interpillar separation. It is therefore not

surprising that a fraction of pillars touch their neighbors and, during continued growth at $T_s=700\text{ }^\circ\text{C}$, merge into broader columns, as discussed below. An example of two pillars touching (and just beginning to merge) is highlighted in the plan-view micrograph in Fig. 3(a) by a dashed square.

IV. DISCUSSION

A competitive growth mode during glancing angle deposition occurs when atomic shadowing, which is exacerbated by the oblique deposition angle, causes a growth instability by favoring the growth of larger pillars at the expense of the smaller ones that die out. This instability is caused by unequal size and/or spacing of the initial surface mounds or the growing pillars and is particularly pronounced for GLAD on flat substrates which leads to a random nucleation of columns.^{28,29} In contrast, growth on regular surface patterns, as done in this study, causes initially no competition between growing pillars, since the nuclei have equal size and spacing as previously reported in Refs. 29 and 31. However, as growth continues, the development of the pillar morphology exhibits variations which can cause the transition to a competitive growth mode. Our results on Ta pillars grown on 260-nm-diameter silica spheres suggest that such a transition occurs at elevated growth temperatures.

The micrographs in Figs. 2–4 and the quantitative analyses presented in Figs. 5 and 6 show clear changes in the pillar morphology as a function of growth temperature. At low T_s , the characteristic length scale for adatom motion is small with respect to the column width.³⁸ Consequently, the column width is not affected by mass transport through surface diffusion, that is, the columns do not broaden due to surface diffusion and their width is controlled only by the shadowing process. Figure 4(a) shows that $T_s=200\text{ }^\circ\text{C}$ leads to pillars with a width, $w=193\pm 14\text{ nm}$, that remains approximately constant as a function of height. This is in agreement with reported simulation results showing that the column radii saturate rapidly and remain constant as a function of column height under purely geometric (i.e., negligible diffusion) conditions.⁴² The pillars are separated by an $\sim 65\text{-nm}$ -wide gap which minimizes growth interactions of neighboring pillars. That is, a stochastic surface modulation that develops on one pillar due to the statistically random deposition process will locally alter the shadowing caused by this pillar but will have negligible effect on the growth of the neighboring pillar, because of their relatively large separation. Consequently, the pillars grow with similar rates and develop into regular arrays that replicate the initial hexagonal surface pattern, as shown in Fig. 2(a).

In contrast, increasing the growth temperature leads to considerable randomness and the regular arrangement of nanopillars completely degrades at $T_s=900\text{ }^\circ\text{C}$, as shown in Figs. 3(b) and 4(b). This is attributed to a transition to a growth mode where column competition dominates the morphological evolution, as discussed in the following. Increasing T_s leads to an increase in the adatom diffusion length which, in turn, results in a pillar broadening. This surface diffusion mediated broadening is quantified in Fig. 5(b),

showing an increase in the average pillar width from 195 nm at $T_s=200$ °C to 260 nm at $T_s=700$ °C. The increase in w is compensated by a decrease in the pillar height [Fig. 5(a)], since the overall mass is conserved. In addition, the increased surface diffusion at elevated T_s is also expected to increase the density within the individual pillars, since surface grooves that would develop into intrapillar voids are filled by diffusing adatoms. A similar pillar broadening and densification has been previously reported, based on both simulation and experimental results,^{30,35} and is also consistent with the structure-zone models for conventional thin films,^{43,44} which predict a densification of columnar morphologies when the homologous temperature T_s/T_m is increased. For the case of Ta, T_s/T_m increases from 0.14 to 0.36 for $T_s=200$ and 900 °C, respectively.

The empty space between neighboring pillars decreases with increasing w . Based on $w(T_s)$ values and the nanosphere diameter, the average gap between pillars along the close-packed direction decreases from ~ 65 nm at $T_s=200$ °C to ~ 0 nm at $T_s=700$ °C. This dramatic decrease results in two competitive growth effects: the extinction and the merging of pillars. Extinct pillars exhibit a smaller height than their neighbors because their growth has terminated prematurely. Examples are highlighted by squares in Figs. 2(b) and 2(c) and arrows in Fig. 4(a). Extinction of pillars is attributed to atomic shadowing which causes larger pillars to capture bigger fractions of the deposition flux than their smaller neighbors. Consequently, the former grow at the expense of their neighbors which die out. This effect is most pronounced when the empty space between the pillars is small, because in that case even small surface morphological irregularities on one pillar can effect the growth on the neighbor. Our experiments support this argument. As the growth temperature increases, the average pillar width increases [Fig. 5(b)], which, in turn, decreases the gap between pillars and causes an increase in the fraction of extinct pillars [Fig. 6(b)]. This observation is consistent with previously reported results, indicating that the growth competition increases with decreasing pattern seed separation.²⁹ The merging of pillars is also directly correlated to their average width. The larger the width, the smaller the gap, and the higher the probability for neighboring pillars to touch and merge. Figure 6(c) shows that the merging probability increases dramatically when T_s reaches 700 °C, since the gap between the pillars approaches ~ 0 nm. The merging of pillars results in agglomerates that, due to their size, capture an overproportional fraction of the deposition flux, leading to exacerbated irregularities and ultimately the breakdown of the regular array structure, as shown in Figs. 3(b) and 4(b). The combination of increased extinction and merging of pillars yields a decrease in the number density of pillars with increasing T_s , as quantified in Fig. 6(a). A similar pillar number reduction with increasing pillar height has been previously observed for GLAD of tungsten and silicon dioxide at 175 °C and has been associated with a competitive growth mode under strong shadowing conditions.³

V. CONCLUSIONS

The surface diffusion strongly affects the morphological evolution of Ta nanopillar arrays during glancing angle deposition on patterned substrates. At low growth temperatures, the nanopillars form regular, hexagonal close-packed arrays, replicating the initial patterns. The pillars are considerably narrower than the center-to-center interpillar distance and their width remains constant. This is attributed to a surface diffusion length which is small with respect to the pillar diameter and to a negligible growth competition associated with a large separation between neighboring pillars.

In contrast, as the growth temperature is increased, the adatom mobility increases, which leads to an increase in the average pillar width. The resulting decrease in space between neighboring pillars leads to a strong interaction of their developing morphologies, due to atomic shadowing effects, and causes a transition to a competitive columnar growth mode. Consequently, some pillars are extinct and others merge with their neighbors, leading to arrays that become increasingly irregular and completely degrade for growth at 900 °C.

ACKNOWLEDGMENT

This research was supported by the National Science Foundation, Division of Manufacturing and Industrial Innovation, under Grant No. DMII-0423358.

- ¹M. Malac and R. F. Egerton, *J. Vac. Sci. Technol. A* **19**, 158 (2001).
- ²K. Robbie, C. Shafai, and M. J. Brett, *J. Mater. Res.* **14**, 3158 (1999).
- ³B. Dick, M. J. Brett, and T. Smy, *J. Vac. Sci. Technol. B* **21**, 23 (2003).
- ⁴M. Malac, R. F. Egerton, M. J. Brett, and B. Dick, *J. Vac. Sci. Technol. B* **17**, 2671 (1999).
- ⁵R. Messier, V. C. Venugopal, and P. D. Sunal, *J. Vac. Sci. Technol. A* **18**, 1538 (2000).
- ⁶Y.-P. Zhao, D.-X. Ye, P.-I. Wang, G.-C. Wang, and T.-M. Lu, *Int. J. Nanosci.* **1**, 87 (2002).
- ⁷S. Kennedy, M. J. Brett, O. Toader, and S. John, *Nano Lett.* **2**, 59 (2001).
- ⁸S. Kennedy, M. J. Brett, H. Miguez, O. Toader, and S. John, *Photonics Nanostruct. Fundam. Appl.* **1**, 37 (2003).
- ⁹J. Wang, H. Huang, S. V. Kesapragada, and D. Gall, *Nano Lett.* **5**, 2505 (2005).
- ¹⁰P. I. Rovira, R. A. Yarussi, R. W. Collins, V. C. Venugopol, A. Lakhtakia, R. Messier, K. Robbie, and M. J. Brett, *Thin Solid Films* **313**, 373 (1998).
- ¹¹I. Hodgkinson, Q. H. Wu, and J. Hazel, *Appl. Opt.* **37**, 2653 (1998).
- ¹²I. Hodgkinson, Q. H. Wu, and S. Collett, *Appl. Opt.* **40**, 452 (2001).
- ¹³G. G. Zhang and Y. P. Zhao, *J. Appl. Phys.* **95**, 267 (2004).
- ¹⁴D.-L. Liu, D.-X. Ye, F. Khan, F. Tang, B.-K. Lim, R. C. Picu, G.-C. Wang, and T.-M. Lu, *J. Nanosci. Nanotechnol.* **3**, 492 (2003).
- ¹⁵M. W. Seto, B. Dick, and M. J. Brett, *J. Micromech. Microeng.* **11**, 582 (2001).
- ¹⁶M. W. Seto, K. Robbie, D. Vick, M. J. Brett, and L. Kuhn, *J. Vac. Sci. Technol. B* **17**, 2172 (1999).
- ¹⁷F. Liu, M. T. Umlor, L. Shen, J. Weston, W. Eads, J. A. Barnard, and G. J. Mankey, *J. Appl. Phys.* **85**, 5486 (1999).
- ¹⁸B. Dick, M. J. Brett, T. J. Smy, M. R. Freeman, M. Malac, and R. F. Egerton, *J. Vac. Sci. Technol. A* **18**, 1838 (2000).
- ¹⁹F. Tang, D.-L. Liu, D.-X. Ye, Y.-P. Zhao, T.-M. Lu, and A. Vijayaraghavan, *J. Appl. Phys.* **93**, 4194 (2003).
- ²⁰A. Lisfi and J. C. Lodder, *Phys. Rev. B* **63**, 174441 (2001).
- ²¹J. P. Singh, G.-R. Yang, T.-M. Lu, and G.-C. Wang, *Appl. Phys. Lett.* **81**, 4601 (2002).
- ²²S. V. Kesapragada, P. Victor, O. Nalamasu, and D. Gall, *Nano Lett.* **6**, 854 (2006).
- ²³A. Lakhtakia, *Mater. Sci. Eng., C* **19**, 427 (2002).

- ²⁴A. Kolmakov and M. Moskovits, *Annu. Rev. Mater. Res.* **34**, 151 (2004).
- ²⁵K. D. Harris, A. Huizinga, and M. J. Brett, *Electrochem. Solid-State Lett.* **5**, H27 (2002).
- ²⁶J. P. Singh, F. Tang, T. Karabacak, T.-M. Lu, and G.-C. Wang, *J. Vac. Sci. Technol. B* **33**, 1048 (2004).
- ²⁷M. J. Colgan and M. J. Brett, *Thin Solid Films* **389**, 1 (2001).
- ²⁸D. Vick, T. Smy, B. Dick, S. Kennedy, and M. J. Brett, *Mater. Res. Soc. Symp. Proc.* **648**, p3.43.1 (2001).
- ²⁹B. Dick, M. J. Brett, T. Smy, M. Belov, and M. R. Freeman, *J. Vac. Sci. Technol. B* **19**, 1813 (2001).
- ³⁰T. Karabacak, J. P. Singh, Y.-P. Zhao, G.-C. Wang, and T.-M. Lu, *Phys. Rev. B* **68**, 125408 (2003).
- ³¹S. V. Kesapragada and D. Gall, *Thin Solid Films* **494**, 234 (2006).
- ³²B. Dick, J. C. Sit, M. J. Brett, I. M. N. Votte, and C. W. M. Bastiaansen, *Nano Lett.* **1**, 71 (2001).
- ³³M. O. Jensen and M. J. Brett, *IEEE Trans. Nanotechnol.* **4**, 269 (2005).
- ³⁴S. Lichter and J. Chen, *Phys. Rev. Lett.* **56**, 1396 (1986).
- ³⁵K. Robbie and M. J. Brett, *J. Vac. Sci. Technol. A* **15**, 1460 (1997).
- ³⁶R. Micheletto, H. Fukuda, and M. Ohtsu, *Langmuir* **11**, 3333 (1995).
- ³⁷C. M. Zhou and D. Gall, *Thin Solid Films* **515**, 1223 (2006).
- ³⁸C. M. Zhou and D. Gall, *Appl. Phys. Lett.* **88**, 203117 (2006).
- ³⁹M. E. Turner, T. J. Trentler, and V. L. Colvin, *Adv. Mater. (Weinheim, Ger.)* **3**, 180 (2001).
- ⁴⁰A. E. Aliev, A. A. Zakhidov, and R. H. Baughman, *Int. J. Nanosci.* **5**, 157 (2006).
- ⁴¹Y. Tatara, H. Sato, and H. Nishikawa, *Proceedings of the Seventh International Conference on Properties and Applications of Dielectric Materials*, 2003, Vol. 1, p. 41.
- ⁴²E. Main, T. Karabacak, and T.-M. Lu, *J. Appl. Phys.* **95**, 4346 (2004).
- ⁴³B. A. Movchan and A. V. Demchishin, *Phys. Met. Metallogr.* **28**, 83 (1969).
- ⁴⁴J. A. Thornton, *Annu. Rev. Mater. Sci.* **7**, 239 (1977).